STABILITY AND FAILURE OF PERFORATED FRIABLE SANDSTONE

Abu. Azam Md.Yassin, Ph.D
Faculty of Chemical Engineering
and Natural Resource Engineering
Universiti Teknologi Malaysia

Introduction

A substantial amount of the world's oil and gas production is from reservoirs of friable nature, in which the rate of production is limited by the risk of formation failure in the completion interval. A failure may stop production either permanently or until an expensive workovers can be carried out. In order to minimize the risk of failure, these formations can be strengthened by gravel packing or through one of several available chemical treatments. However, such strengthening measures are expensive and may restrict production or complicate future recompletions to alternative intervals.

Knowledge of completion strength is essential for selecting the optimum type of completion and evaluating the need for a strengthening treatment. The completion decision will be based largely on the maximum allowable sand-free production rate for each candidate completion interval. The completion strength depends on the inherent strength of the formation rock and the stresses imposed on the rock during production. The stresses near the completion depend on many factors including flow rate, well pressure, reservoir pressure and the original in-situ state of stress.

Literature Review

Formation sands having no strength of cementation between sand grains can be stabilized by arches of sand that form around each perforation opening. Some theoretical works has been published on the stability of these arches while producing fluids from the formation.

Bratli and *Risnes*[1] developed a model by stress analysis on a spherical cavity. They put forward a stability criterion relating the flow forces and the strength parameters in the plastic zone. Their assumptions of spherical cavity is due to the *trap door* configuration of their experiment where gravity forces tend to make the arch spherical.

Nordgren[2] similar put forward a failure criterion based on stress analysis in hemispherical cavity. His criterion of failure at yield point is too conservative since it had been shown that sandstone surpassed yield point without failure[3]. But his assumption of hemispherical cavity is consistent with laboratory's[4,5] observation based on downhole configuration.

Stein and *Hilchie*[6] and later *Stein, Odeh* and *Jones*[7] developed method based on the projection of *safe* and *fail* production rates from a test well to another wells located in a given area by assuming drawdown or pressure gradient that cause instability in any well is proportional to the sand strength or shear modulus.

For formation with some strength of cementation, tunnels are formed when initially perforated. Some theoretical works[8,9] has been published on the stability of these tunnels under confining pressure but no works dealing with stability of these tunnels under formation fluids production is available.

The present works is intended to provide a basic theoretical understanding of the mechanical stability of a perforation tunnel in a friable formation during fluid production from the formation.

Model Description

The geometry of the model is as illustrated in Figure 1. It shows a horizontal perforation tunnel through a porous and permeable rock connected to a borehole with the inside radius, R_1, the midpoint distance between two adjacent perforation tunnels, R_0 and the perforation length, L. Axial symmetry around the tunnel is assumed and also the rock is assumed isotropic and homogeneous with the pores completely filled with fluid. A plain strain deformation condition is assumed.

Condition of plasticity around a perforation tunnel

The production oil, gas and/or water from an underground reservoir results in a local change in the stress and strain field in a porous, permeable material surrounding the tunnel due to change in pore pressure. For friable sandstone formation the elastic limit can be surpassed without the actual failure.

When critical stresses are reached, the material will be transformed from an elastic to a plastic state. At the transition point, this relation will be the *Mohr-Coulomb* criterion. But with increasing deformation, the strength of the material may be reduced further, and the constants C and N may be a function of the

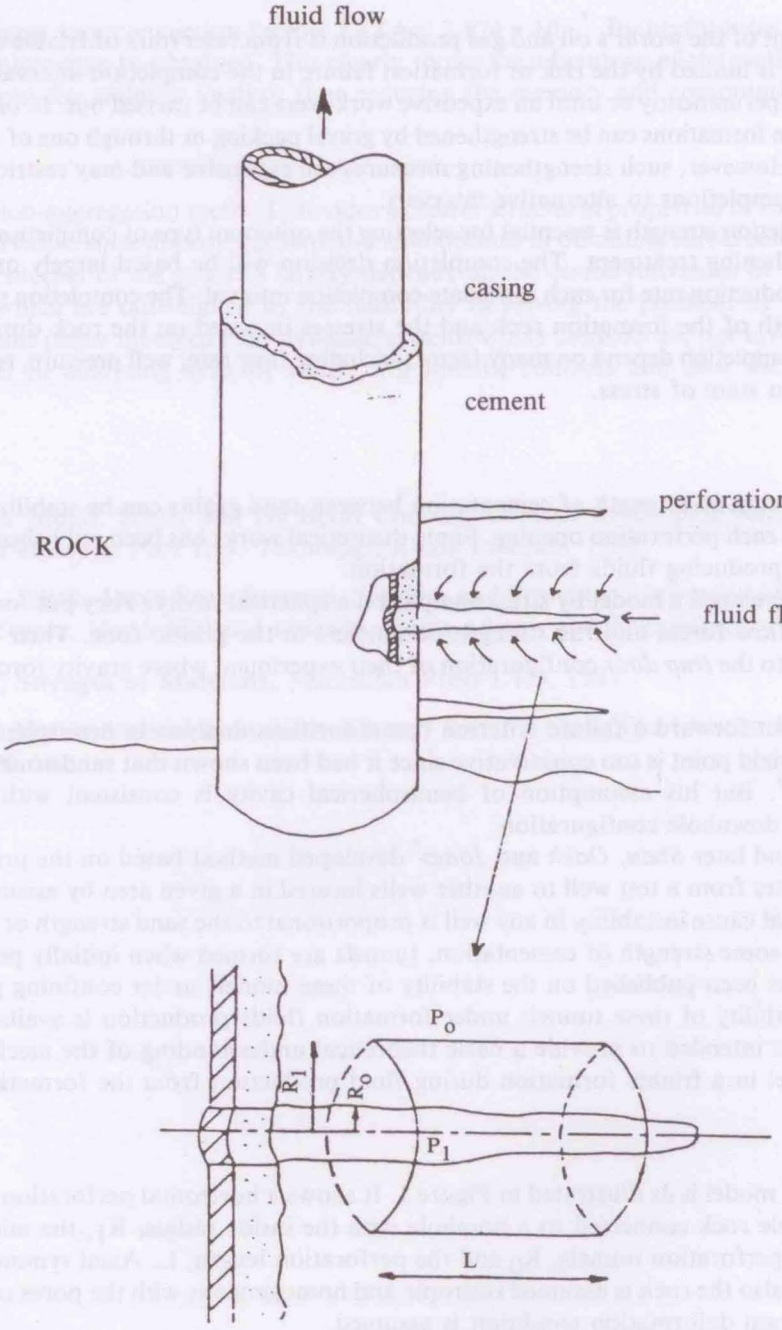

Figure 1 Configuration of Perforation Tunnel Problem

degree of deformation and possibly dependent upon the previous history of the material. Also, in the real case there will be a gradual transition from the elastic to the plastic state.

However, for simplicity consider an ideal material which behaves elastically up to the limit given by the *Mohr-Coulomb* criterion. The parameters C and N may have different values from the ones used in the elastic zone but they are assumed constant for a given material.

Stress around a perforation tunnel plastic state[10]

This distribution of stresses around the perforation tunnel is governed by the force equilibrium equation in the plastic zone.

$$\frac{\delta \sigma_r}{\delta_r} + \frac{\sigma_r - \sigma_\theta}{r} = 0 \qquad \ldots (1)$$

At the plastic-elastic interface, the relationship between the principal stresses governed by the *Mohr-Coulomb* yield criterion equation.

$$f = \delta_\theta - \delta_r N^2 + (N^2 - 1)\, p - 2CN = 0 \qquad \ldots (2)$$

Assuming a constant flow of fluid into the perforation tunnel, the fluid pressure, p can be expressed by *Darcy's* law as

$$p = \frac{\mu Q}{2\pi LK_a} \ell n \frac{r}{R_1} + P_1 \qquad \ldots (3)$$

The flow rule associated with (2) is

$$\varepsilon_r^P = K \frac{\delta f}{\delta \sigma_r} = -KN^2, \; \varepsilon_\theta^P - K \frac{\delta f}{\delta \sigma_\theta} = K, \; \varepsilon_z^P = K \frac{\delta f}{\delta \sigma_z} = 0 \qquad \ldots (4)$$

where, $\varepsilon_r^P, \varepsilon_\theta^P, \varepsilon_z^P$, is the plastic strain components and K is a scalar.
From (4) it follows that

$$\varepsilon_r^P + \varepsilon_\theta^P N^2 = 0 \qquad \ldots (5)$$

And total strain component is defined as

$$\varepsilon_r = \varepsilon_r^e + \varepsilon_r^p, \varepsilon_\theta = \varepsilon_\theta^e + \varepsilon_\theta^p, \varepsilon_z = \varepsilon_z^e + \varepsilon_z^p \qquad \ldots (6)$$

The relationship relating stress and elastic strain is given by:

$$\begin{aligned} E\varepsilon_\theta^e &= \sigma_r - \upsilon(\sigma_\theta + \sigma_z) - (1 - 2v)\ \beta p \\ E\varepsilon_\theta^e &= \sigma_\theta - \nu(\sigma_r + \sigma_z) - (1 - 2v)\beta p \\ 0 &= \sigma_z - \nu(\sigma_z + \sigma_\theta) - (1 - 2v)\beta p \end{aligned} \qquad \ldots (7)$$

By combining (2) with (5), (6) and (7) and substituting the resulting expression with the strain-displacement equation into (1) lead to the displacement equation

$$2Gu = A_1 r^{N2} + A_2 r^{-N2} + A' r + A'' r \ln r \qquad \ldots (8)$$

where: A_1 and A_2 are integration constants and

$$A' = \frac{2(1 - 2v)}{N^4 - 1}(1 - \beta) + \frac{N^2}{N^2 + 1} + \frac{(1 - 2v)}{N^2 - 1} - \nu \frac{\mu Q}{2\pi L K_a}$$

$$A'' = (1-2\nu)(1-\beta)\frac{\mu Q}{2QLK_a}$$

The stress distribution around a perforation tunnel can be found by solving (8) for the strain relationships and inserting the resulting expression into (7) with (5), (6) and (3). Combining these solutions with the boundary condition

$$\sigma_r = p_i \quad \text{at } r = R_i$$

the final solution for the stress components are given as

$$\sigma_r = P_i + \frac{\mu Q}{2\pi LK_a} \ln \frac{r}{R_i} + \frac{1}{t}\left(2CN - \frac{\mu Q}{2\pi LK_a}\right)\left(\frac{r}{R_i}\right)^t - 1 \qquad \ldots (9)$$

$$\sigma_\theta = P_1 + \frac{\mu Q}{2\pi LK_a}\left(1 + \ln \frac{r}{R_1}\right) + \frac{1}{t}\left(2CN - \frac{\mu Q}{2\pi LK_a}\right)(t+1)\left(\frac{r}{R_1}\right)^t - 1 \qquad \ldots (10)$$

Extend of Plasticity around a perforation tunnel

If failure is expressed in terms of the limiting extension of the plastic zone to the midpoint distance between two adjacent perforation tunnels or any specified distance from the centre of the perforation tunnels as determined by experimental testing of core, then the conditions for failure can be obtained.

At the plastic-elastic interface, the *Mohr-Coulomb* yield criterion hold. Another requirement is continuity in the radial stress across the boundary. When the radial stress from the plastic region (9) and the tangential stress from the elastic zone is inserted into the *Mohr-Coulomb* yield criterion (2), the resulting equation in R_c is

$$C_1 R_c^{\,t-2} \ln R_o/R_c + C_2 R_c^{\,t} \ln R_o/R_c + C_3 R_c^{\,3} + C_4 R_c^{\,2} \ln R_c/R_i + C_5 R_c^{\,2}$$

$$\ln R_o/R_c + C_6 \ln R_o/R_c \ln R_c/R_i + C_7 \ln R_o/R_c + C_8 \ln R_o/R_c + C_9 = 0 \qquad \ldots (11)$$

where:

$$C_1 = \left(2CN - \frac{\mu Q}{2\pi LK_a}\right) R_1^{-t}$$

$$C_2 = \frac{t+2}{t} C_1 R_o^2$$

$$C_3 = -\frac{(1-2\nu)}{2(1-2\nu)} \beta (P_0 - P_1)$$

$$C_4 = \frac{(1-2\nu)}{2(1-\nu)} \beta \frac{\mu Q}{2\pi LK_a}$$

$$C_5 = \frac{\mu Q}{2\pi LK_a}$$

$$C_6 = -\left(2 - \frac{1-2\nu}{1-\nu}\beta\right) C_5 R_o^2$$

$$C_7 = -C_4 R_o^2$$

$$C_8 = (2\sigma_{RO} - (P_0 - P_1)\ \beta \frac{(1-2v)}{(1-v)} - 2P_1 + \frac{2}{t}(2CN) - \frac{t+2}{t}\ \frac{\mu Q}{2\pi LK_a}\ R_o^2$$

$$C_9 = -C_3 R_0^2$$

Result And Discussion

The example used to illustrate the model developed is given in Table 1.

Table 1 Parameters used for Calculation

At formation of 10,000 ft:

Pore pressure gradient	=	0.465 psi/ft
Formation pressure gradient	=	0.95 psi/ft
Perforation diameter	=	0.5 ins
Perforation shots/ft	=	4 for 0° phasing
Formation angle	=	30°
Formation strength	=	217 psi
Formation compressibility	=	1.0
Poisson's ratio	=	0.26
Flowrate/perforation	=	10b/d
Perforation length	=	12 ins
Fluid viscosity	=	0.8 cp
Formation permeability	=	100 mD
Plastic zone permeabillity	=	70 mD
Skin zone permeability	=	10 mD
Extent of skin (damage)	=	0.35 ins from centre of tunnel

Stress Distribution around a Perforation Tunnel with no Fluid Flow

The condition of no fluid flow into the perforation tunnel normally assumes that the fluid pressure in the perforation is in balance with the pore pressure in the formation. This would correspond to the situation immediately following the perforating operation.

The distribution of stresses is shown in Figure 2. This thickness of the plastic region in this case extends approximately 0.7 ins from the centre of the tunnel. As long as there is no fluid flow, the thickness of the plastic region depends primarily on the original in-situ stress, pore pressure, the perforation configuration and the formation parameters.

Stress Distribution around a Perforation Tunnel under Flowing Condition

This condition corresponds to fluid production from the reservoir into the wellbore through the perforations. The distribution of stresses under flowing conditions is shown in Figure 3. The thickness of the plastic zone increases when compared with the no flow condition assumed in Figure 2. Under flowing conditions, the thickness of the plastic zone is dependent upon the same parameters as the no flow condition and in addition those parameters associated with fluid flow.

Maximum Sandfree production rate

Figure 4 shows the maximum sand-free flowrate attainable before perforation tunnel failure occurs. Failure resulted from the expansion of the plastic zone towards the midpoint distance of adjacent perforations or any specified distance from the centre of the tunnel.

Stability analysis

The concept of stability ratio is introduced to facilitate the determination of failure. Stability ratio (SR) is defined as the ratio of the radius of the plastic zone to a specified distance from the centre of the tunnel.

The effect of the parameters on the SR are plotted for a specified flowrate through the perforation and failure occurs when a specified SR is exceeded. This limit can be determined according to the range of formation encountered and the operational requirements.

The effect upon the SR of both the extent and the properties of the compacted zone around the perforation

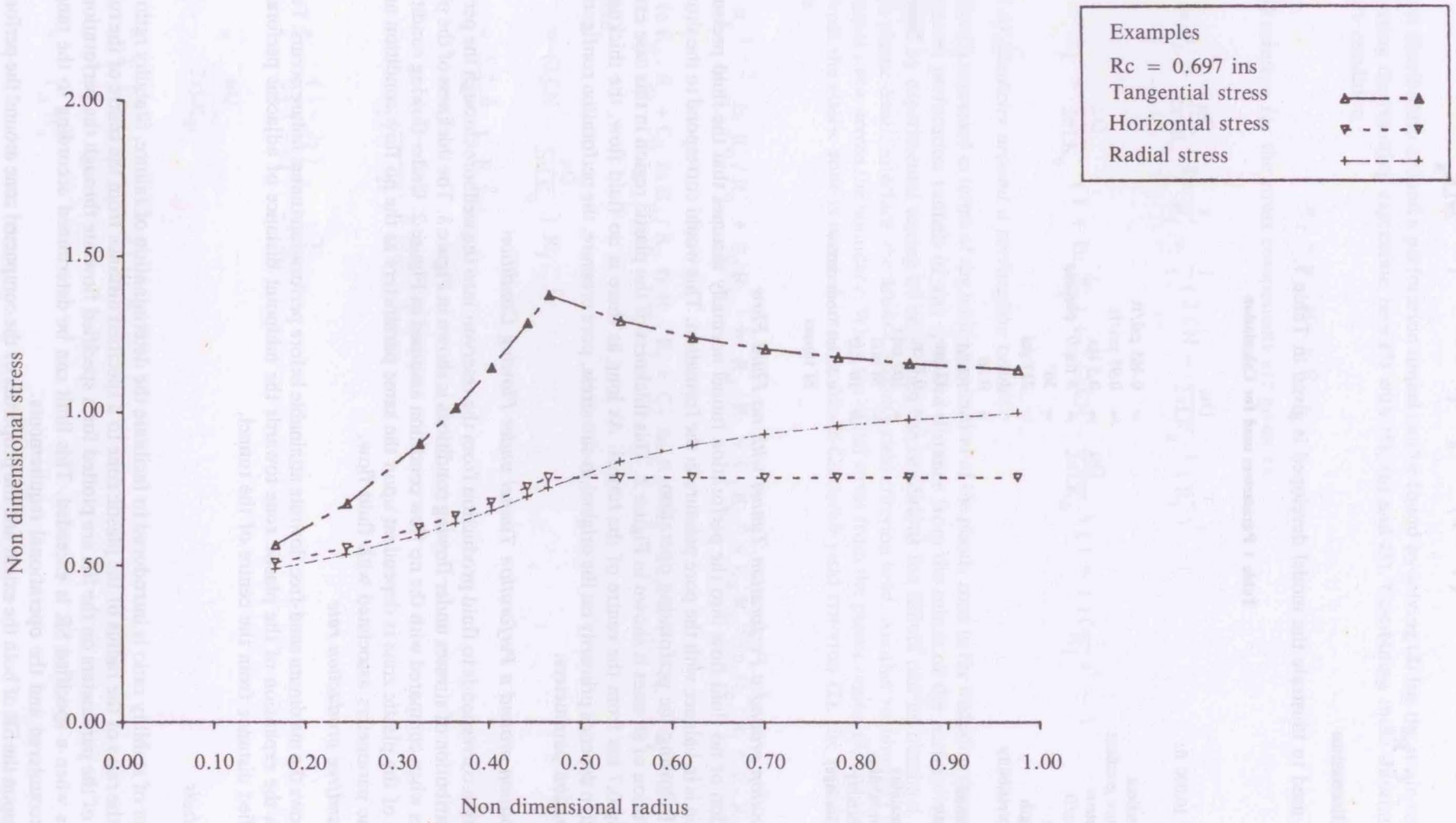

Figure 2 Distribution of Stress in Perforation Tunnel (No. Flow Condition, Elstic-Plastic State)

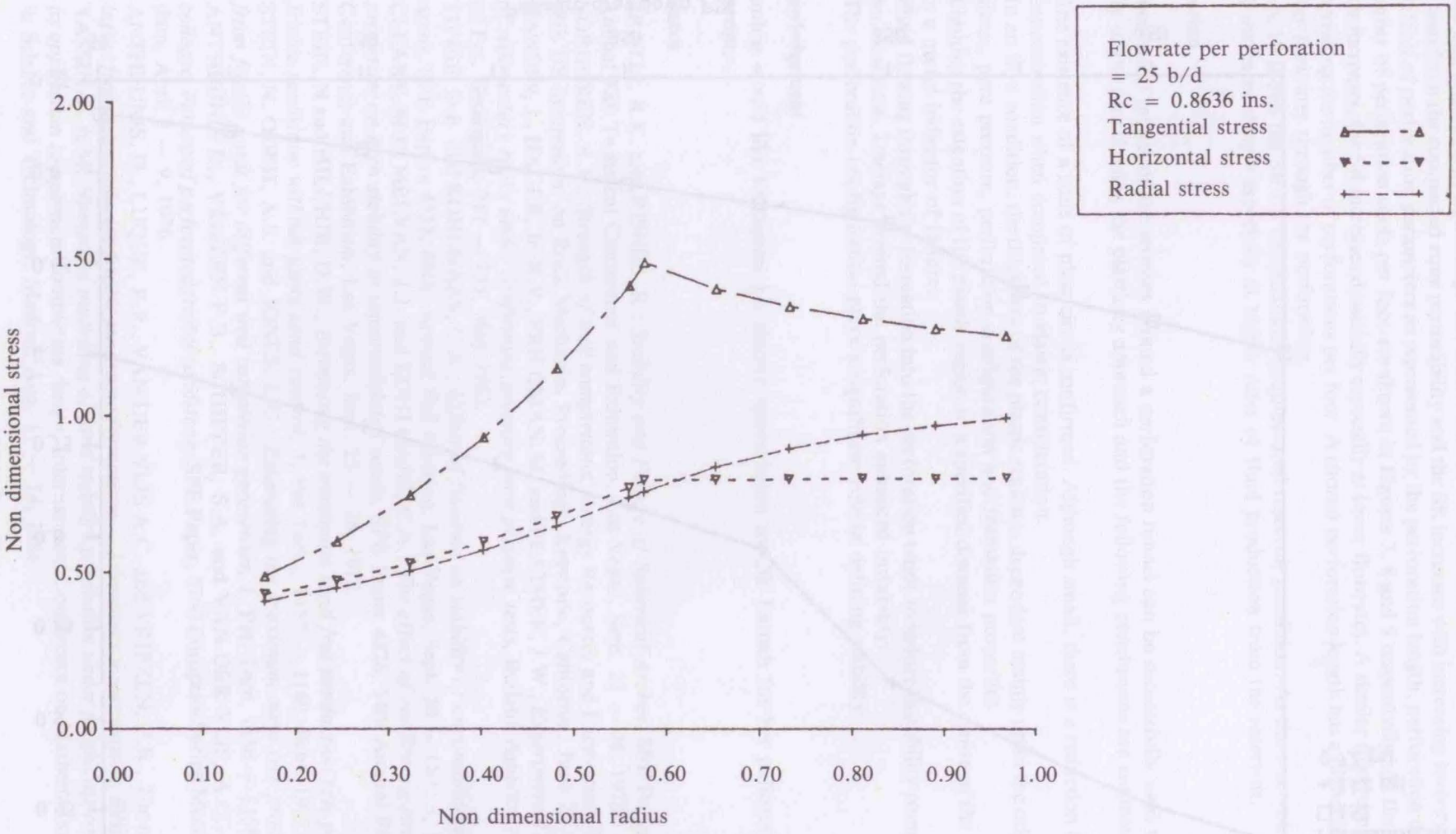

Figure 3 Distribution of Stresses in Perforation Tunnel (Flowing Condition, Elastic-Plastic State)

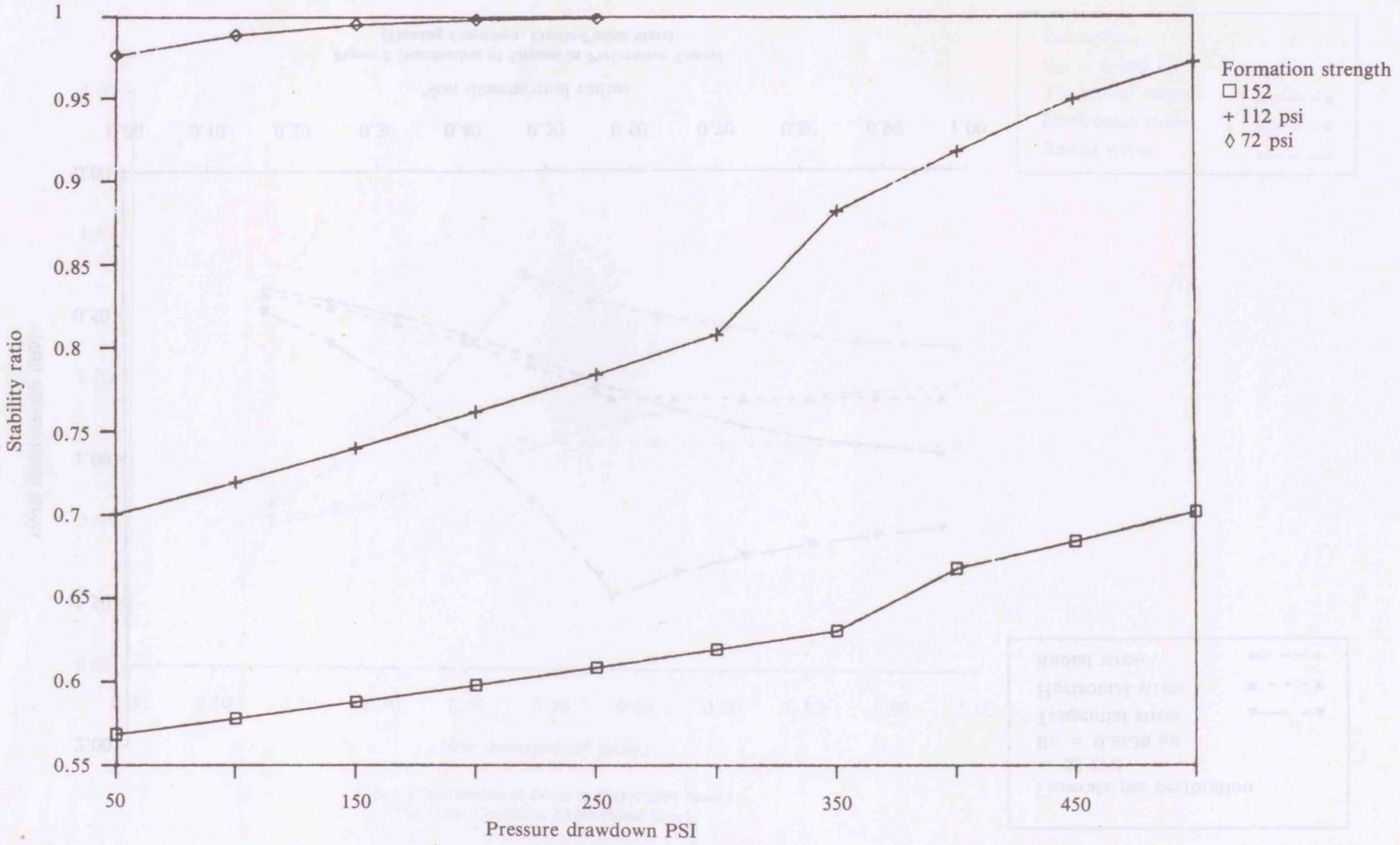

Figure 4 Maximum sand free flowrate per perforation tunnel

tunnel are shown in Figure 5 and 6, respectively. As the depth of the compacted zone increases the SR increases and higher flowrate through the tunnel tend to increase the SR further. The degree of damage can be seen from the compacted zone permeability and the SR increases with increasing severity of damage.

The effect of perforation parameters as represented by the perforation length, perforation diameter and the number of perforation shots per foot are shown in Figures 7, 8 and 9 respectively: As the perforation diameter increases, the SR increases drastically especially at lower flowrates. A similar trend can be observed with increasing the number of perforations per foot. A shorter perforation length has a higher SR especially at higher flowrates through the perforation.

Figure 10 shows the SR for depleted and geopressured reservoir condition. As the reservoir is depleted the SR increases steeply especially at higher rates of fluid production from the reservoir.

Conclusion

This theoretical model of the stresses around a perforation tunnel can be successfully used to study the stability of the tunnel using the plasticity approach and the following conclusions are enumerated below:

(a) The existence of a zone of plasticity is confirmed. Although small, there is a reduction of the stress concentration when compared to elastic consideration.
(b) In no flow condition, the thickness of the plastic region is dependent mainly upon the original in-situ stress, pore pressure, perforation configuration and formation properties.
(c) Limiting the extention of the plastic region to a specified distance from the centre of the perforation is a useful indicator of failure.
(d) Fluid flowing through the formation into the perforation tends to induce instability compared to the no flow case. Damage around the perforation enhanced instability.
(e) The perforation configuration plays a significant role in defining stability.

Acknowledgement

The author would like to express his sincere appreciation to Cik Latnah for her patience typing this manuscript.

References

1. BRATLI, R.K. and RISNES, R.; *Stability and Failure of Spherical Arches,* SPE Paper 8427, 54th Annual Fall Technical Conference and Exhibition, Las Vegas, Sept. 23 — 26, 1978.
2 NORDGREN, R.P., *Strength of well completions,* Energy Resources and Excavation Technology, 18th US Symposium on Rock Mechanics Proceedings, Keystone, California, June 22 — 24, 1977.
3 HANDIN, J., HAGER, Jr. R.V., FRIEDMAN, M. and FEATHER, J.W., *Experimental deformation of sedimentary rocks under confirming pressure pore pressure tests,* Bulletin American Association of Pet. Geologists, 717 — 755, May 1963.
4 TIPPIE, D.B. and KOHLHAAS, C.A.; *Effect of flowrate on stability of unconsolidated producing sands,* SPE Papers 4533, 48th Annual Fall Meeting, Las Vegas, Sept. 30 — Oct. 3, 1973.
5 CLEARY, M.P, MELVAN, J.J. and KOHLHAAS, C.A.; *The effect of confirming stress and fluid properties on arch stability in unconsolidated sands,* SPE Paper 4826, 54th Annual Fall Technical Conference and Exhibition, Las Vegas, Sept. 23 — 26, 1978.
6 STEIN, N and HILCHIE, D.W., *Estimating the maximum sand free production rate possible from friable sandstone without using sand control,* J. Pet Tech., 1157 — 1160, Sept. 1972.
7 STEIN, N. ODEH, A.S. and JONES, L.G.; *Estimating the maximum sand free production rates from friable sands for different well completion geometries,* J. Pet. Tech, 1156 — 1158, Oct. 1974.
8 ANTHEUNIS D., VRIEZEN P.B., SCHIPPER, S.A. and VAN DER VLIS, A.C., *Perforation collapse: Failure of perforated friable sandstone,* SPE Paper, 5750 European Spring Meeting, Amsterdam, April 8 — 9, 1976.
9 ANTHEUNIS, D., LUQUE, R.F., VAN DER VLIS A.C. and VRIEZEN, P.B., *The onset of sand influx from gas producing friable sandstone formations — laboratory investigations,* SPE Paper 8021.
10 YASSIN, A.A.M, *Numerical modelling of sand stability prediction under producing conditions and its application to optimum completion design,* International Conference on Mathematical Modelling in Science and Technology, Madras, Aug. 11 — 14, 1988.

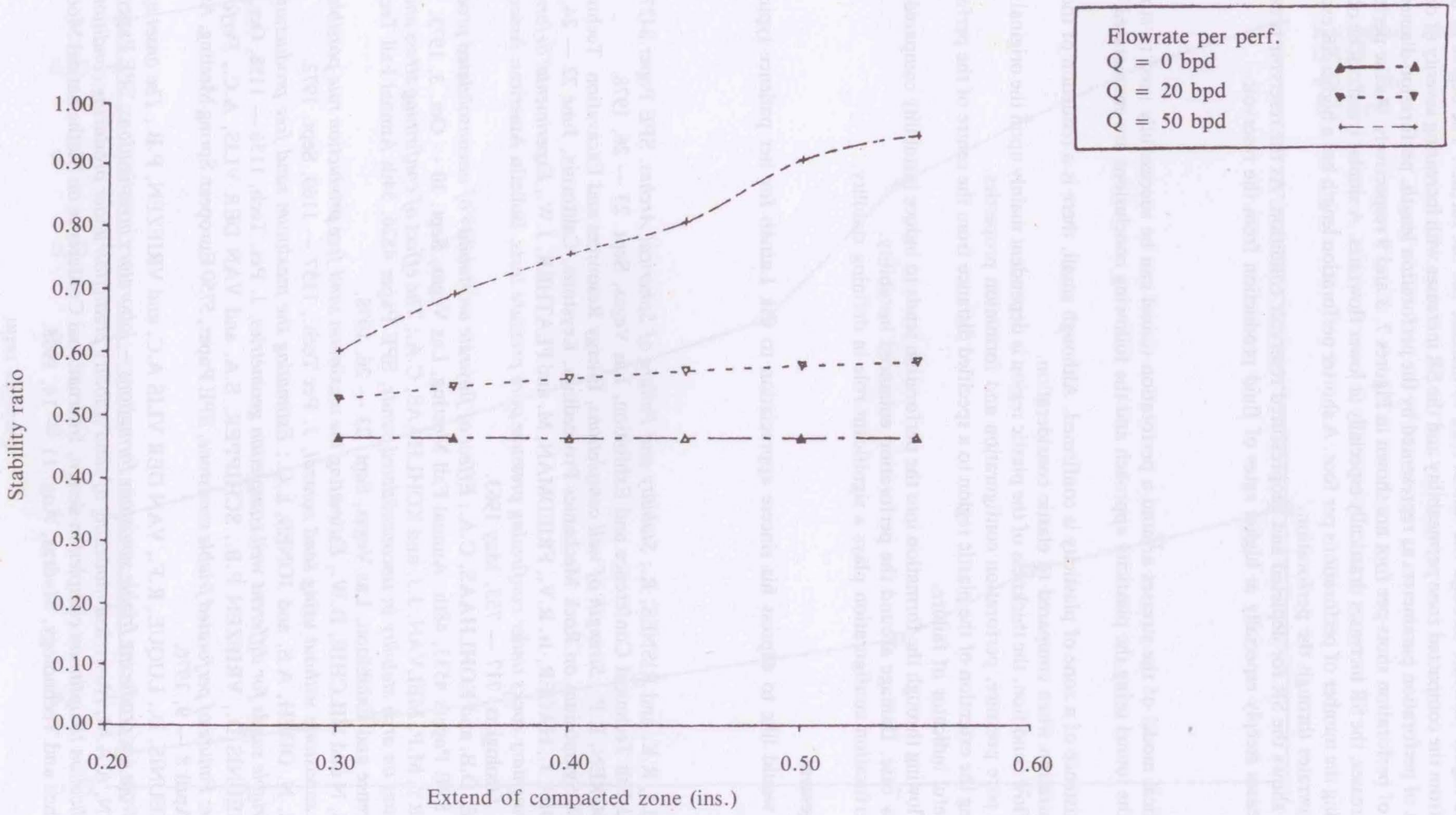

Figure 5 Stability Ratio vs Extend of Compacted Zone at Various Flowrate

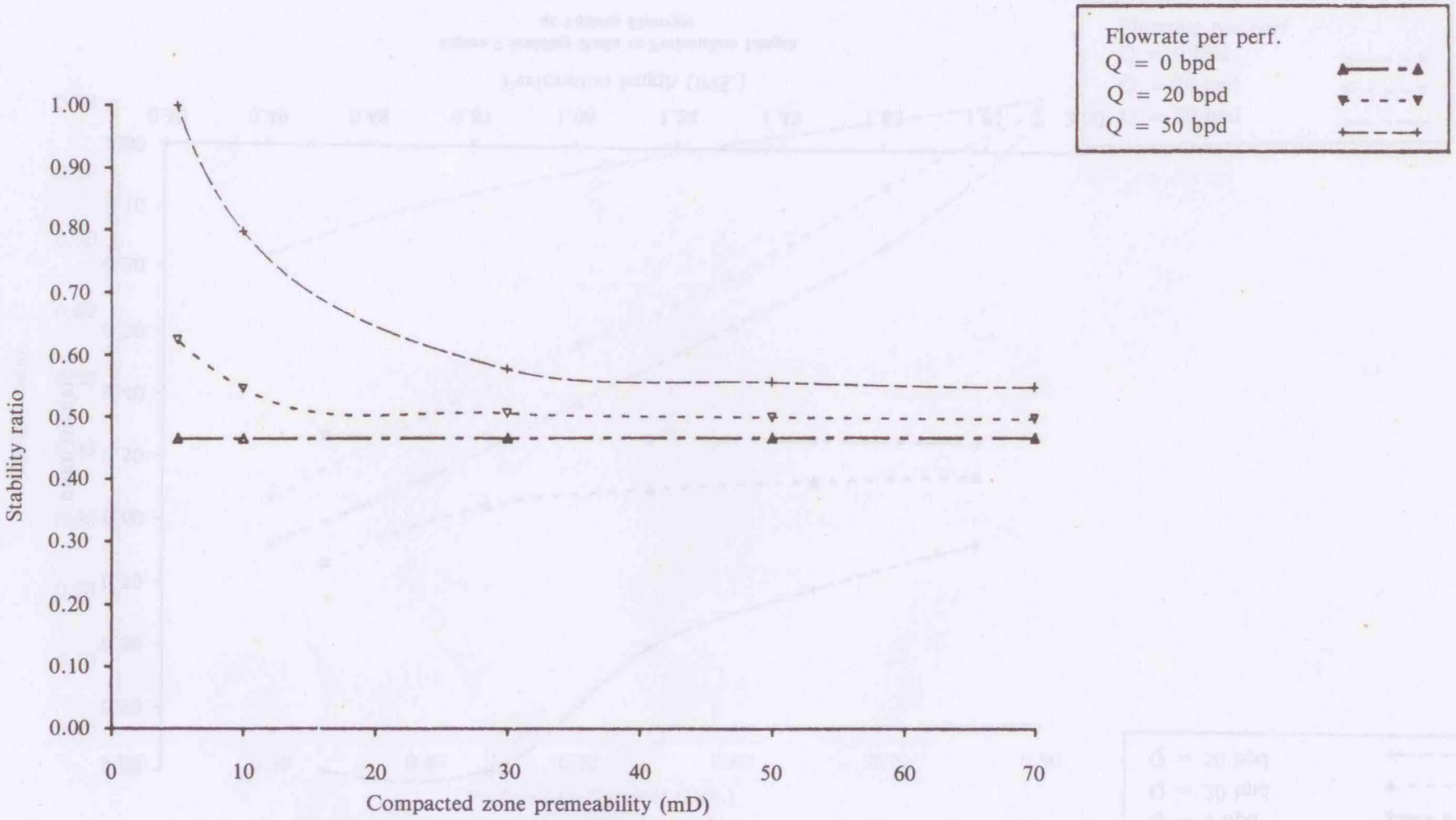

Figure 6 Stability Ratio vs Compacted Zone Permeability at Various Flowrate

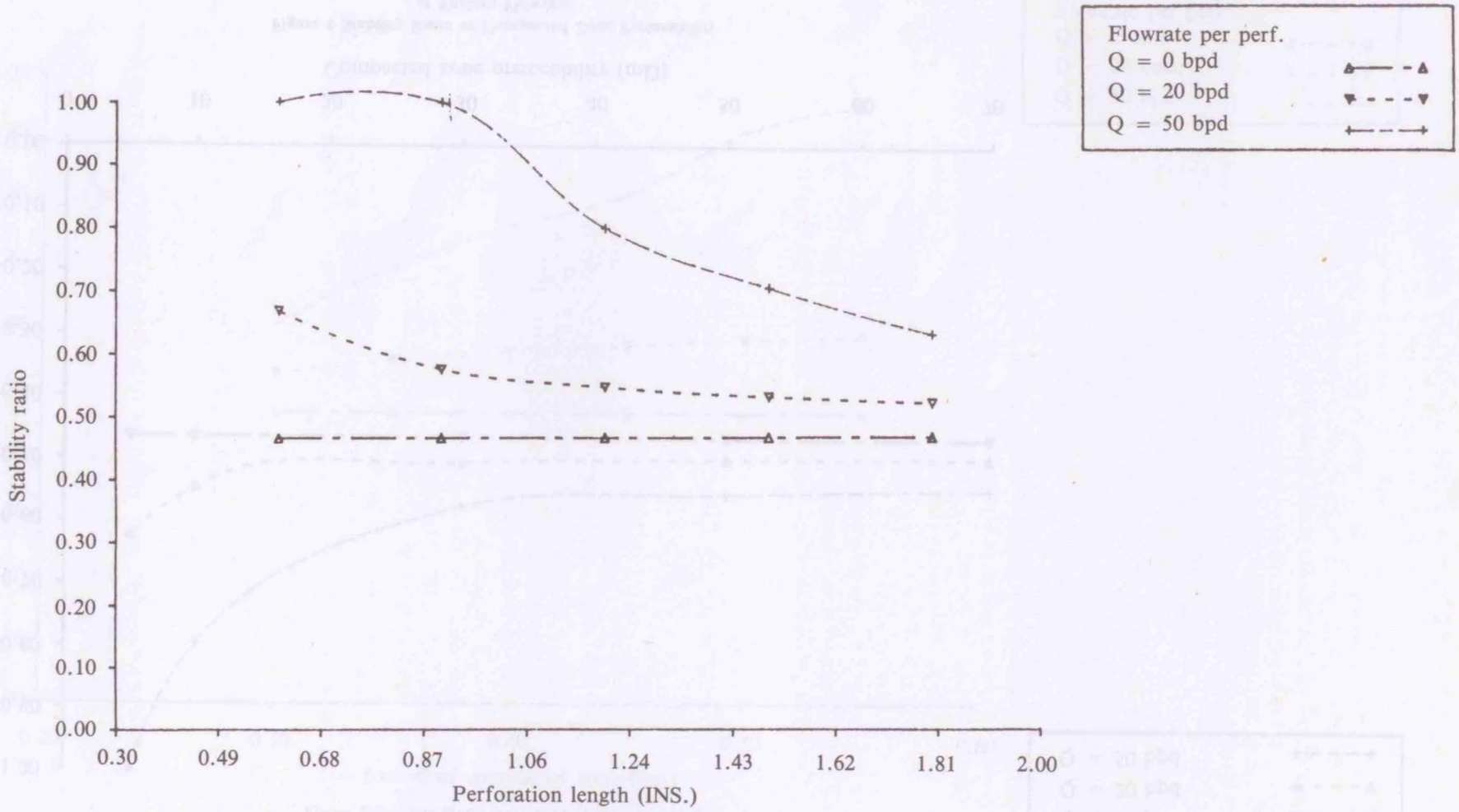

Figure 7 Stability Ratio vs Perforation Length at Various Flowrate

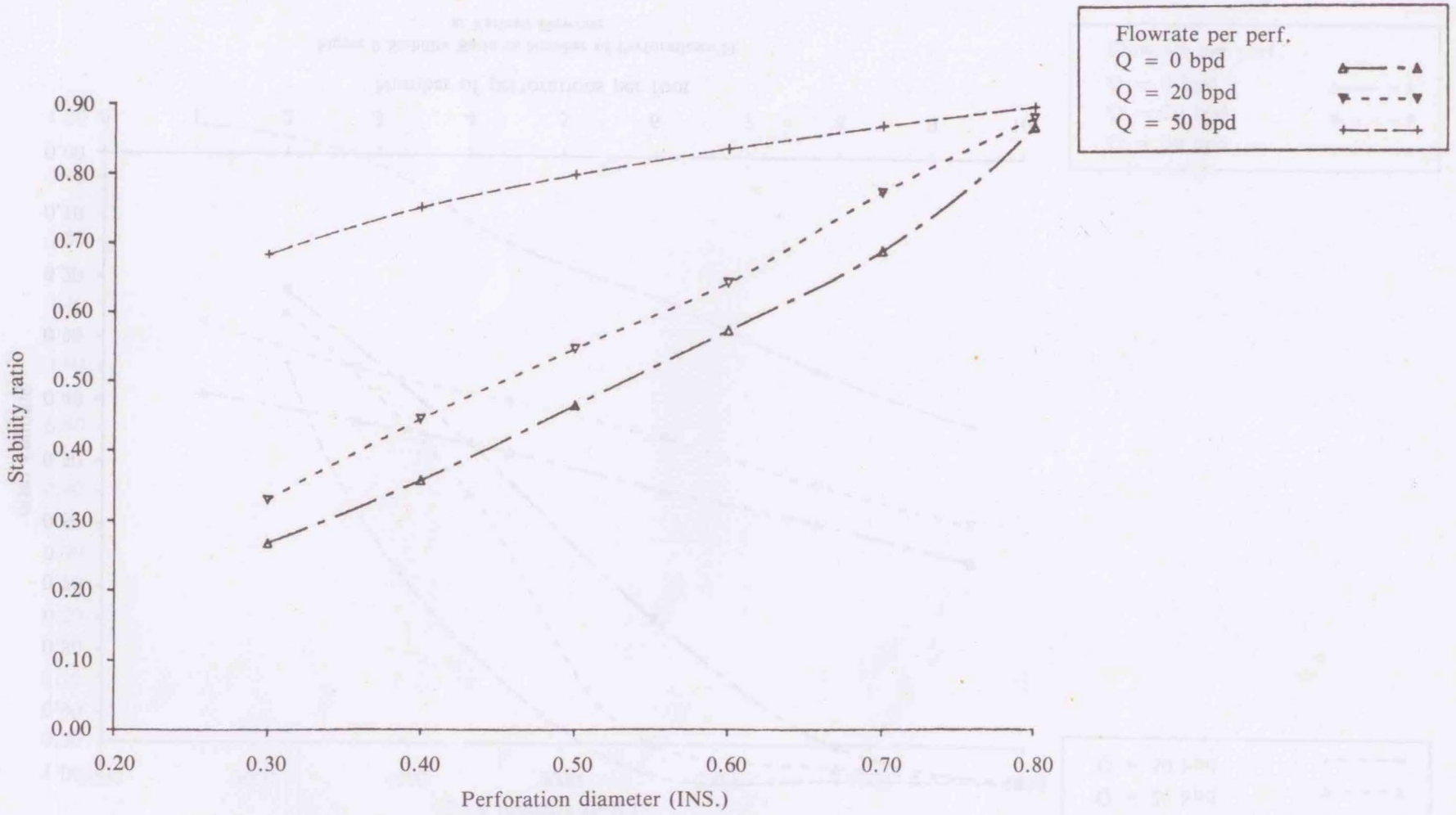

Figure 8 Stability Ratio vs Perforation Diameter at Various Flowrate

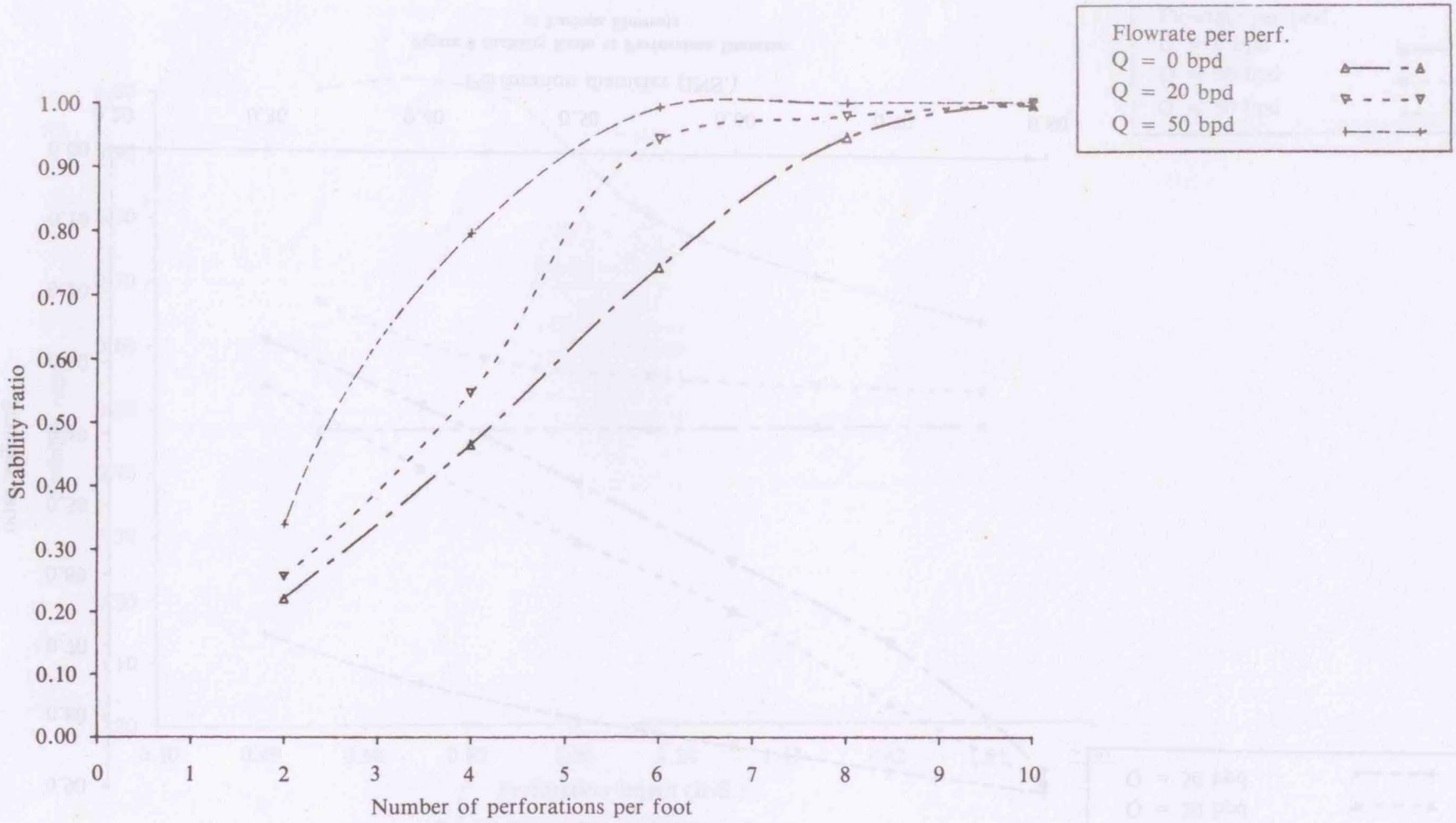

Figure 9 Stability Ratio vs Number of Perforations/Ft at Various Flowrate

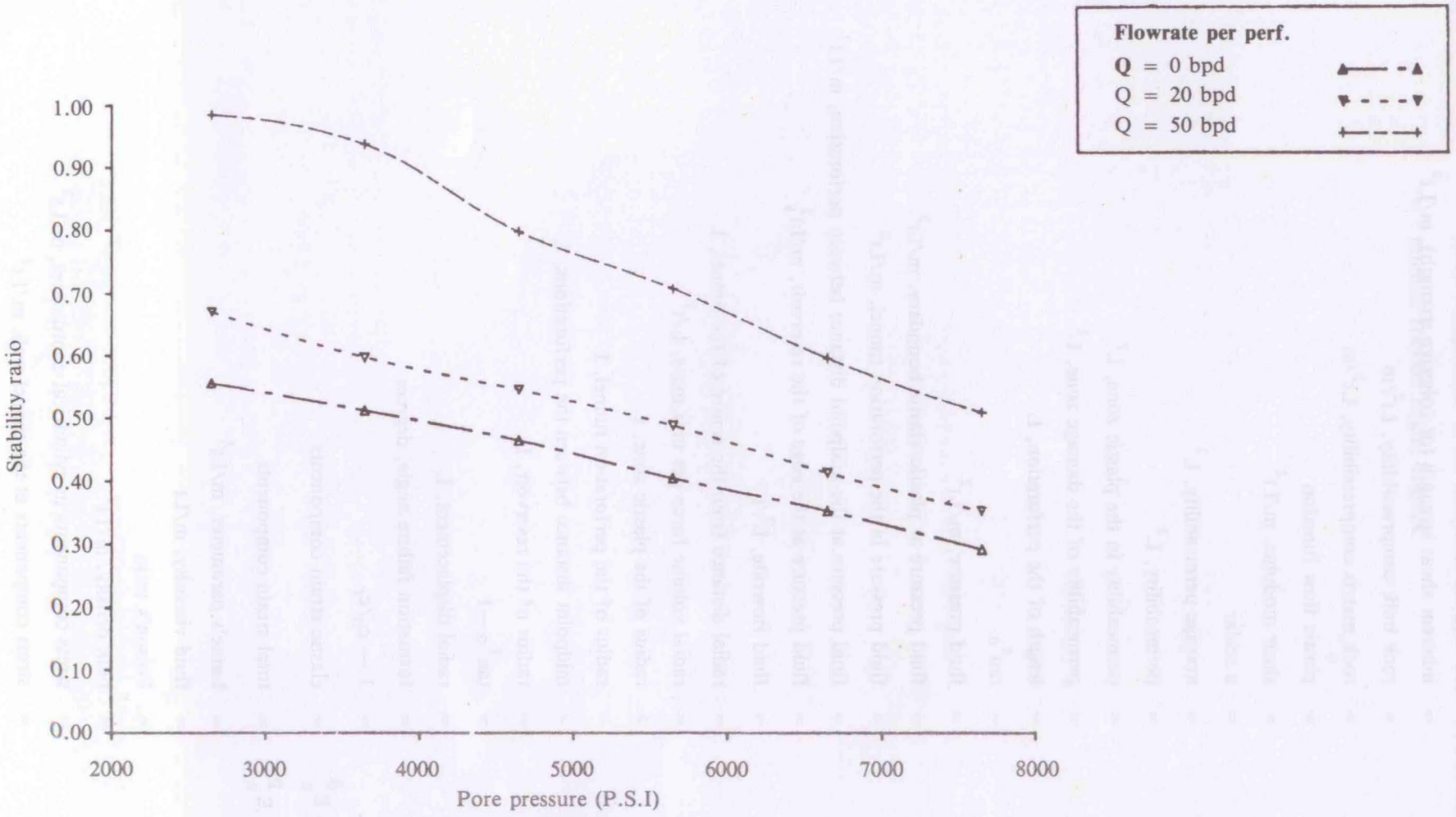

Figure 10 Stability Ratio vs Pore Pressure at Various Flowrate

Nomenclature

c	=	inherent shear strength (or cohesive strength), m/Lt^2
c_b	=	rock bulk compressibility, Lt^2/m
c_r	=	rock matrix compressibility, Lt^2/m
f	=	plastic flow function
G	=	shear modulus, m/Lt^2
K	=	a scalar
K_a	=	average permeability, L^2
k	=	permeability, L^2
k_c	=	permeability in the plastic zone, L^2
k_s	=	permeability of the damage zone, L^2
L	=	length of the perforation, L
N	=	$\tan^2\alpha$
p	=	fluid pressure, m/Lt^2
p_c	=	fluid pressure at plastic/elastic boundary, m/Lt^2
p_i	=	fluid pressure in the perforation tunnel, m/Lt^2
p_o	=	fluid pressure at the midpoint distance between perforation, m/Lt^2
p_r	=	fluid pressure at the edge of the reservoir, m/Lt^2
Q	=	fluid flowrate, L^3/t
r	=	radial distance from the centre of the tunnel, L
R	=	radial volume force per unit mass, L/t^3
R_c	=	radius of the plastic zone, L
R_i	=	radius of the perforation tunnel, L
R_o	=	midpoint distance between the perforations, L
R_R	=	radius of the reservoir, L
t	=	$\tan^2\alpha - 1$
u	=	radial displacement, L
α	=	formation failure angle, degrees
β	=	$1 - c_b/c_r$
ε_r^θ , $\varepsilon_\theta^\theta$, ε_z^θ	=	elastic strain components
ε_r^p , ε_θ^p , ε_z^p	=	total strain components
γ	=	Lame's parameter, m/Lt^2
μ	=	fluid viscosity, m/Lt
υ	=	Poison's ratio
ρ	=	bulk density, m/Lt^3
σ_r , σ_θ , σ_z	=	stress components in cylindrical coordinates, m/Lt^2
σ_{R1}	=	stress components at the tunnel wall, m/Lt^2

σ_{RC} = stress components at the plastic/elastic boundary, m/Lt^2

σ_{RD} = stress components at the midpoint distance between perforations, m/Lt^2

ϕ = internal friction angle, degrees.